Central Lancashire Online Knowledge (CLoK)

Title	Spectrochemical analyses of growth phase-related bacterial responses to low (environmentally-relevant) concentrations of tetracycline and nanoparticulate silver
Type	Article
URL	https://clok.uclan.ac.uk/id/eprint/21321/
DOI	https://doi.org/10.1039/C7AN01800B
Date	2018
Citation	Jin, Naifu, Semple, Kirk T., Jiang, Longfei, Luo, Chunling, Zhang, Dayi and Martin, Francis L (2018) Spectrochemical analyses of growth phase-related bacterial responses to low (environmentally-relevant) concentrations of tetracycline and nanoparticulate silver. The Analyst. ISSN 0003-2654
Creators	Jin, Naifu, Semple, Kirk T., Jiang, Longfei, Luo, Chunling, Zhang, Dayi and Martin, Francis L

It is advisable to refer to the publisher's version if you intend to cite from the work.
https://doi.org/10.1039/C7AN01800B

For information about Research at UCLan please go to http://www.uclan.ac.uk/research/

Spectrochemical analyses of growth phase-related bacterial responses to low (environmentally-relevant) concentrations of tetracycline and nanoparticulate silver

Naifu Jin[1], Kirk T. Semple[1], Longfei Jiang[2], Chunling Luo[2], Dayi Zhang[1,3,*], Francis L. Martin[4,*]

[1]*Lancaster Environment Centre, Lancaster University, Lancaster LA1 4YQ, UK;*

[2]*Guangzhou Institute of Geochemistry, Chinese Academy of Sciences, Guangzhou 510640, China;*

[3]*School of Environment, Tsinghua University, Beijin 100084, China;*

[4]*School of Pharmacy and Biomedical Sciences, University of Central Lancashire, Preston PR1 2HE, UK;*

*Corresponding authors:

Francis L Martin, School of Pharmacy and Biomedical Sciences, University of Central Lancashire, Preston PR1 2HE, UK; Email: flmartin@uclan.ac.uk

Dayi Zhang, School of Environment, Tsinghua University, Beijin 100084, China; Email: d.zhang@lancaster.ac.uk

Abstract

Exposure to environmental insults generally occurs at low levels, making it challenging to measure bacterial responses to such interactions. Additionally, microbial behaviour and phenotype varies in differing bacterial types or growth phases, likely giving rise to growth- or species-specific responses to environmental stimuli. The present study applied a spectrochemical tool, infrared (IR) spectral interrogation coupled with multivariate analysis, to investigate the growth- and species-specific responses of two bacterial strains, Gram-negative *Pseudomonas fluorescens* and Gram-positive *Mycobacterium vanbaalenii*, to low concentrations of tetracycline, nanoparticulate silver (AgNP) or mixtures thereof. Results indicate the tendency for tetracycline-induced biospectral alterations to occur in outer-cellular components, *e.g.*, phospholipids or proteins, while AgNPs-induced changes are mainly associated with proteins (~ 964 cm^{-1}, ~ 1485 cm^{-1}, ~ 1550 cm^{-1}, ~ 1650 cm^{-1}). The primary altered targets are correlated with bacterial membranes or outer-cellular components. Furthermore, significant lipid changes at 1705-1750 cm^{-1} were only present in *P. fluorescens* cells compared to *M. vanbaalenii*, owing to differences in cell wall structure between Gram-positive and -negative bacteria. This study also found distinct biospectral alterations in non-log phase compared to log phase, confirming bacterial growth-dependent responses to environmental exposures. It implies that previous studies on log phase only may underestimate the impacts from exposures of interest *in situ*, where bacteria stay in different growth stages. Our work proves the feasibility of biospectroscopy in determining bacterial responses to low-level environmental exposures in a fast and efficient manner, revealing sufficient biochemical information continuously through growth phases. As a nondestructive approach, biospectroscopy may provide deeper insights into the actual and *in situ* interactions between microbes and environmental stimuli, regardless of the exposure level, growth phase, or bacterial types.

50   **ToC graphic**

51

52

53
54
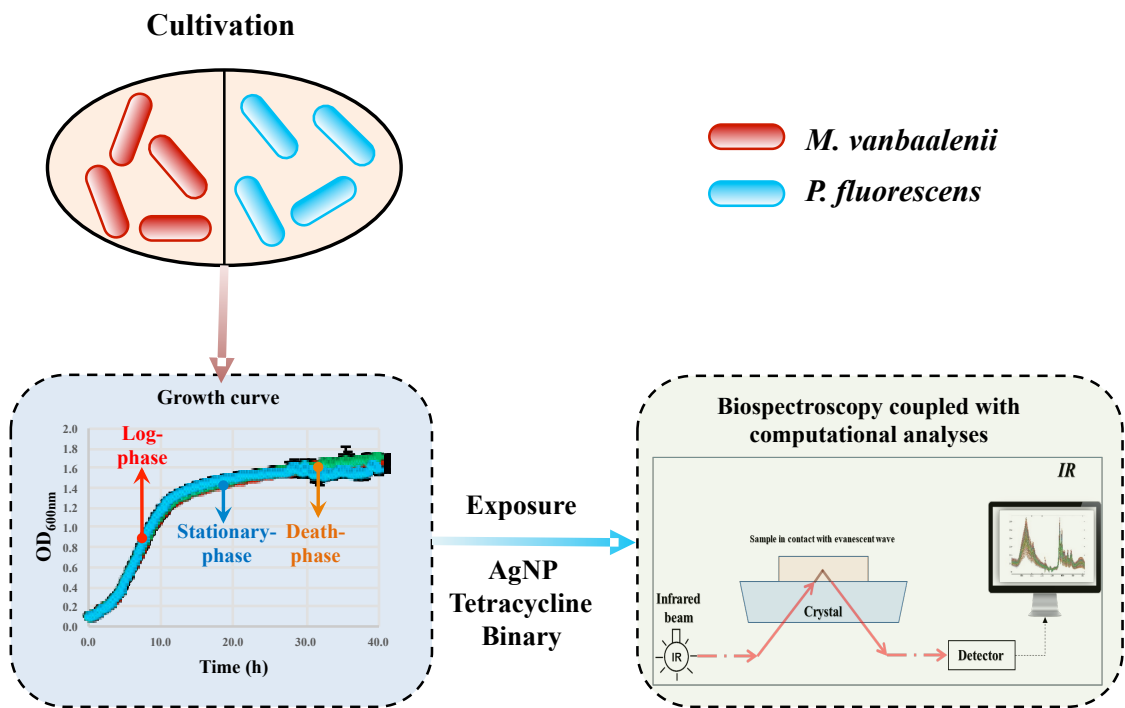
Introduction

The impacts of environmental insults on microorganisms have been widely studied. Antibiotics are a group of antimicrobial agents capable of causing environmental insults of major concern from both a scientific and public perspective. A significant number and quantity of antibiotics have been extensively applied in human and veterinary medicine[1]. Various means by which these drugs and their metabolites enter the environment post-excretion have been examined. The most common way by which antibiotics are discharged is *via* sewage treatment plants with ultimate release into surface or groundwater. Previous studies point to >40 different categories of antibiotics found in groundwater and even drinking water, ranging from nanogram per liter to microgram per liter[1-4]. Strikingly, residues of veterinary antibiotics enter the environment in a much more direct way through application of liquid manure as fertilizer[5, 6].

Additionally, nanoparticles (NPs) may also pose high risks to our living environment. Nanoparticulate silver (AgNP) is one of the most widely-used NPs, occurring in analytical pathogen-detecting devices, as antibacterial additives in commercial products (clothing, food containers, wound dressings, implant coatings, and refrigerators), and in ultrafiltration membranes for water purification[7-9]. The abuse and widespread usage of antibiotics and AgNPs may exacerbate risks of antimicrobial resistance[10]. Although many studies have addressed such consequences in living microorganisms, they usually employ very high-level exposures of antibiotics and AgNPs in the laboratory, generally 100- or even 1000-fold greater than exposures in real-world scenarios. Thus, the *in-vitro* outcome of high-level exposure in reflecting real-world impacts is always questioned[11, 12].

Bacteria play a critical role in geochemical processes and are ubiquitously present in the environment as a unique group of microorganisms. They can be used advantageously to study the impacts of environmental exposures, but their communities are incredibly complicated with regards to composition, functions and dynamics[13-16]. Gram staining depending on cell membrane structure, for instance, is the general classification method for categorizing bacteria into Gram-positive or -negative groupings. The fundamental difference between these two categories is membrane structure, *i.e.*, there is only a thin peptidoglycan layer (~2-3 nm) between the cytoplasmic membrane and the outer membrane of Gram-negative bacteria while

88   Gram-positive bacteria exhibit a thick peptidoglycan layer of 30 nm but lack an outer

89   membrane[17]. Differing attributes of membrane structure may result in distinct

90   responsive behaviors towards environmental exposures, for instance towards toxicity

91   and anti-biocide actions[18]. Additionally, growth phase is another major concern in

92   studying bacterial communities. Bacterial growth is typically divided *via* growth rate,

93   *i.e.*, lag phase, acceleration phase, exponential phase (log-phase), retardation phase,

94   stationary phase, and phase of decline. In previous studies, log-phase has been the

95   most investigated, but this condition is seldom found in the natural environment due

96   to rarity of optimal growth conditions[19]. Instead, stationary- to death-phase

97   representing nutrient depletion circumstances may be more representative[20].

98   To date, a wide range of techniques have been used to assess bacterial responses

99   to environmental exposures, such as Christensen test-tube method (CTT)[21, 22], Congo

100   red agar method (CRA)[23], IcaADB gene detection using polymerase chain reaction

101   (PCR)[24, 25], and pulsed-field gel electrophoresis (PFGE)[26, 27]. However, these

102   approaches target specific endpoints and are not feasible for diagnosing bacterial

103   responses to environmental exposures. CTT and CRA primarily require access to pure

104   cultures. The others are molecular-based, defining the genotype of a whole

105   community rather than the individual phenotype or behavior. For instance,

106   distinguishing the functions or behaviours of individual bacterial cells within a

107   bacterial biofilm is almost impossible *via* molecular-based methods, owing to the

108   enormous diversity of bacterial strains and complexity in community structure.

109   Additionally, these approaches have to be performed under restrictive laboratory

110   conditions[28-30], making it unachievable to discriminate bacterial phenotypes within

111   complex bacterial communities in real environmental samples. Therefore, an

112   increasing need for novel high-throughput approaches is raised, allowing one to

113   analyze the real environmental microbiota *in situ via* a non-destructive means.

114   Biospectroscopy has a long history of application in microbiology since the

115   1960s[31, 32]. Attributes of biospectroscopy include non-destructive, non-invasive,

116   high-throughput and label-free, which provide many advantages for the investigation

117   of environmental and biochemical dynamic changes in low-level exposure

118   circumstances. In recent studies, biospectroscopy has proved sensitive to

119   physiological and morphological alterations resulted from low-level environmental

120   exposures[33-35]. Specifically, infrared (IR) spectroscopy exploits the principle that

5

121 biochemical bonds perform some degree of vibrations induced by stretching, bending,

122 scissoring or twisting after energy absorption at particular wavelengths. The

123 "biochemical-cell fingerprint" region is located within the mid-IR region, which is the

124 most information-rich about biochemical structures[36]. Through assessing derived

125 spectral peaks or alterations, *i.e.*, bio-fingerprints, the biochemical structure of

126 interrogated targets can be revealed[37-39]. Additionally, Raman spectroscopy, as a

127 complementary method to IR, can provide information on chemical bonds and

128 composition even under a hydrated environment[40, 41]. Furthermore, another merit of

129 biospectroscopy over other techniques is that it allows investigations to be undertaken

130 *in situ* in real-time, which can generate continuous biochemical information through

131 the entire biological processes rather than only obtaining static results from specific

132 time points.

133   As a broad-spectrum of antibiotic, tetracycline is effective against both Gram-

134 positive and -negative bacteria with only a few exceptions[42], having a history of

135 several decades usage in animal feeds and consequently probably more ubiquitous in

136 the natural environment than other in-house antibiotics (*e.g.*, kanamycin)[43]. The

137 present study therefore chose tetracycline as the studied antibiotic, discriminating and

138 assessing bacterial responses to tetracycline and AgNPs *via* biospectroscopy coupled

139 with multivariate analysis. Additionally, recent studies have reported the synergistic

140 antibacterial effects of antibiotics and metals or NPs[44], *e.g.*, amoxicillin and AgNPs [45],

141 but its effects on bacterial physiology remains unclear. Our work also considered and

142 interrogated microbial responses to the binary-exposure of tetracycline and AgNPs *via*

143 IR spectroscopy. Regarding the real-world scenario, our results distinguished the

144 distinct biospectral alterations in different bacterial types and growth phases, helping

145 one to understand the bacterial behaviour post-exposure to low-level antimicrobials.

146 We aim to demonstrate that biospectroscopy approaches can characterise

147 physiological features of bacteria and lend profound insights into the relationship

148 between these and bacterial responses to environmental insults.

149

Materials and methods

Sample preparation

Unless stated otherwise, all the chemicals used in this study were purchased from Sigma-Aldrich (UK). The AgNPs (catalogue no. 730785, Sigma-Aldrich, UK) have a 10-nm particle size at a stock concentration of 0.02 mg/mL, dissolved in aqueous buffer with sodium citrate as stabilizer. Two classic soil bacterial strains, *Mycobacterium vanbaalenii* PYR-1 (Gram-positive) and *Pseudomonas fluorescens* (Gram-negative), were selected owing to their ubiquity and wide distribution in the soil environment and their well-known physiological behaviour[36, 46-48]. These two strains were cultured in Luria-Bertani (LB) broth at $30\pm2^{\circ}C$ with 150 rpm shaking for 24 h. Bacterial growth was measured every 10 min by optical density at 600 nm (OD_{600}) with a microplate reader (FLUOstar Omega, BMG Labtech, UK). AgNPs, tetracycline or AgNPs-tetracycline mixture was added into cell suspensions in early log-phase ($OD_{600}=0.6$), respectively. To mimic the low-level exposure in natural environment[49-52], the exposure concentration was set as 4 μg/L for AgNPs and 1 μg/L for tetracycline. One millilitre of bacterial suspension was taken 2, 8 and 24 h post-exposure, representing log-phase, stationary-phase and death-phase, respectively. For each sample, bacterial cells were harvested by centrifugation at 4000 relative centrifugal force (rcf) for 5 min, and the cell pellets were subsequently washed three times with sterile deionized water and 70% ethanol to fix bacteria and remove residues of growth media. The fixed samples were then applied onto Low-E slides for subsequent spectrochemical analysis.

Spectrochemical analysis

IR spectra were acquired *via* a Bruker TENSOR 27 FTIR spectrometer (Bruker Optics Ltd., UK) equipped with a Helios ATR attachment containing a diamond internal reflection element (IRE). Instrument parameters were set at 32 scans and 16 cm^{-1} resolution. A total number of 30 spectra were acquired per sample through the ATR magnification-limited viewfinder camera. Before measuring each new specimen, the crystal was cleaned with deionized water, and background readings were retaken.

Raman spectra were acquired *via* an InVia Renishaw Raman spectrometer (Renishaw Inc. Gloucester, Gloucestershire, UK). After calibration, sample slides were placed on an operating stage (a Renishaw automated 100 nm encoded XYZ

182 stage), and a 50× objective (numeral aperture 0.75) was applied to focus on the cell

183 pellet. The parameters of measurement included: grating scan type (extended);

184 spectrum range (400 to 1800 cm^{-1}); configuration (Laser, 785 nm edge); grating (1200

185 l/mm 633/790); exposure time (30 s); accumulations (1); and, laser power (100%).

186 When all the parameters were set up, a map measurement was used for analyzing each

187 colony. The spectrometer's entrance slit of 50 μm combined with a 1200 lines/mm

188 (~1.0 cm^{-1} spectral resolution) diffraction grating dispersing Raman signals onto a

189 master Renishaw Pelletier cooled charge coupled detector (CCD). A white light

190 camera mounted on the microscope was used to obtain the darkfield images and

191 visualize locations for spectral acquisition. For each captured picture of a cell pellet,

192 25 spectra were randomly obtained.

193 *Spectrochemical data processing*

194 All the initial data generated from ATR-FTIR spectroscopy were analyzed using

195 MATLAB R2011a (TheMathsWorks, Natick, MA, USA) coupled with the IRootLab

196 toolbox (http://irootlab.googlecode.com)[53]. The acquired IR spectra were cut to the

197 biochemical-cell fingerprint region (1800 - 900 cm^{-1}), undertaken rubberband baseline

198 correction and normalized to Amide I (1650 cm^{-1}). Multivariate analysis of principal

199 component analysis-linear discriminant analysis (PCA-LDA) was applied to the

200 pre-processed data to derive ten uncorrelated principal components (PCs) from

201 acquired spectra, which account for >99% of the total variance and also maximize

202 inter-class variance whilst minimizing intra-class variance[54-56]. Cross-calculation was

203 subsequently performed to mitigate risk resulting from LDA overfitting[57]. The

204 PCA-LDA loadings using (n-1) samples (n = number of samples in dataset) was

205 trained *via* leave-one-out cross-validation and then calculated the scores of the rest

206 sample. This process was performed for all scores within the test. To investigate roles

207 of reactive oxygen species (ROS) in antibiotic action and resistance, the

208 CySS-to-protein ratio was calculated from derived Raman spectra by dividing the

209 intensity of cysteine band (CySS, 668 cm^{-1}) by that of protein band (1447 cm^{-1})[34].

210 *Statistical analysis*

211 Statistical significance of differences and variance analysis (*P*-value <0.05) of

212 biospectral alterations among different treatments of bacterial types and growth

213 phases was performed using one-way analysis of variance (ANOVA) with Tukey's

214   post-hoc test. All statistical analyses were carried out in GraphPad Prism 6.

215   Multivariate regression trees (MRT) were used to analyze the influence of bacterial

216   type, growth phase and exposure on biospectral alterations using the R package

217   "mvpart". Herein, Gram-positive (*M. vanbaalenii*) and Gram-negative (*P. fluorescens*)

218   strains were assigned as 1 and 0. For growth phase, the log-phase, stationary-phase,

219   and death-phase were assigned as 1, 2 and 3, respectively. The exposure of AgNPs,

220   tetracycline and their mixtures were assigned as 1, 2 and 3, respectively.

221

Results and discussion

222

223   *Growth curves post-exposure to AgNPs and tetracycline*

224   Growth curves (Figure 1) for *M. vanbaalenii* (Figure 1A) and *P. fluorescens* (Figure

225   1B) show that both strains exhibit approximately a 3 h lag-phase and the log-phase

226   starts some 3.5 h after initial culture. Both enter the stationary-phase at approximately

227   11 h (OD_{600}=1.2). After about 30 h culture, significant fluctuations indicate the death

228   phase stage for both strains. There was no significant difference regarding the growth

229   between control (non-exposure) and exposure groups (P >0.05). Although previous

230   work reports a remarkable inhibition of bacterial growth post-exposure to AgNPs[58],

231   the exposure levels herein (4 ng/mL) are much lower than the previous study (10-100

232   μg/mL) and it therefore appeared not to significantly impact either bacterial strain.

233   Similarly, low concentrations of tetracycline did not induce any apparent changes on

234   the respective growth curves either. A previous study reports that *Synechocystis* sp.

235   exposure to 1 μg/L of tetracycline for five days exhibited no apparent effect, possibly

236   because of natural variability in tetracycline resistance[59]. Additionally, *M. vanbaalenii*

237   and *P. fluorescens* are both environmental bacteria widespread in natural habitats

238   (water and soil), and they are reported to tolerate insults from low-level exposures of

239   antimicrobials[36]. Thus, their growth curves are hardly affected by low-level exposures

240   to AgNPs or tetracycline.

241   *Growth-dependent spectrochemical alterations derived from IR spectra*

242   Raw spectra reveal very limited information because low-level exposures may only

243   induce miniscule alterations (Figure 1C and 1D). Multivariate analysis assists in

244   highlighting the spectral changes and key distinguishing biomarkers representing

245 spectral differences. Previous studies indicate that most features align along linear

246 discriminant one (LD1), which includes most of the spectral information (Figure 2)[34,

247 36]. The observed segregation in PCA-LDA scores plots (Figure 2A and 2E) is

248 significant (P <0.05), indicating distinct biospectral alterations between the growth

249 phases. The results of one-way ANOVA [see Electronic Supporting Information (ESI)

250 Table S1 and S2] also demonstrate the statistically significant means of all

251 segregation categories in each growth phase (P <0.05).

252 Biospectral discriminant peaks and their tentative assignments illustrate the

253 interactions between cellular components in different growth stages (Figure 3). The

254 spectra of *M. vanbaalenii* show a broad range of variations in stationary-phase

255 compared to log-phase (Figure 3A), including glycogen (~1018 cm^{-1}), carbohydrate

256 (~1165 cm^{-1}), symmetric phosphate stretching vibrations ($v_sPO_2^-$; ~1088 cm^{-1}), COO-

257 symmetric stretching vibrations of fatty acids and amino acid (~1377 cm^{-1}), lipid

258 (~1701 cm^{-1}), and proteins (~1474 cm^{-1})[60]. The main discriminant peaks in

259 death-phase include Amide I (~1650 cm^{-1}), Amide II (~1550 cm^{-1}), glycogen (~1018

260 cm^{-1}), and proteins (~1481 cm^{-1})[36, 60]. In contrast, the major spectral features of *P.*

261 *fluorescens* are identical in stationary-phase and death-phase (Figure 3E), mainly

262 comprising proteins and lipids, *i.e.*, Amide I (~1650 cm^{-1}), Amide II (~1550 cm^{-1}),

263 and lipids (1705-1750 cm^{-1})[34, 35]. For both strains, the degrees of all the

264 growth-related alterations illustrate an increasing tendency from stationary-phase to

265 death-phase, possibly attributed to cellular differentiation under nutrient depleted

266 conditions in stationary-phase and death-phase, which cause the changing cell wall

267 structure to adapt to growth circumstances[20, 61, 62]. The spectral differences between

268 the two strains is principally contributed by cell membrane structure in that

269 Gram-negative bacteria contain two lipid-associated bilayers compared to

270 Gram-positive cells[17]. The extra membrane in Gram-negative strains (*P. fluorescens*)

271 might increase more detectable alterations related to proteins and lipids across growth

272 phases.

Spectrochemical alterations with AgNPs/tetracycline exposure

274 Although the exposures herein are low-level, characterizable effects can be identified

275 post-exposure to AgNPs, tetracycline or their mixtures *via* biospectrsocopy coupled

276 with multivariate analysis. The key alterations in *M. vanbaalenii* post-exposure to

277 AgNPs include glycogen (~1022 cm^{-1}), proteins (~1485 cm^{-1}), $v_sPO_2^-$ (~1088 cm^{-1},

278   1092 cm^{-1}), carbohydrate (~1165 cm^{-1}), lipids (~1705 cm^{-1}, 1709 cm^{-1}), Amide I

279   (~1670 cm^{-1}), and protein phosphorylation (~964 cm^{-1}) (Figure 3B)[33, 36]. Tetracycline

280   exposure led to discriminating alterations in *M. vanbaalenii* in Amide III (~1269

281   cm^{-1}), protein phosphorylation (~964 cm^{-1}), glycogen (~1022 cm^{-1}), Amide I (~1609

282   cm^{-1}, 1612 cm^{-1}, 1659 cm^{-1}), COO- symmetric stretching vibrations of fatty acids

283   and amino acid (~1408 cm^{-1}), and lipids (~1701 cm^{-1}, 1713 cm^{-1})[60] (Figure 3C).

284   However, for *P. fluorescens*, the biomarkers in both individual treatments are further

285   concentrated on proteins (~1650 cm^{-1}, ~1550 cm^{-1}) and lipids (1705-1750 cm^{-1})[34, 36]

286   (Figure 3F and 3G).

287   In binary exposure treatments, more complex profile differences in spectral

288   alterations in ATR-FTIR spectra are observed. The primary changes in *M.*

289   *vanbaalenii* are consistent with proteins (~1650 cm^{-1}) and lipids (1705-1750 cm^{-1}) in

290   all growth phases (Figure 3D)[34, 36]. In contrast, the exposure-associated spectral

291   alterations in *P. fluorescens* vary significantly with growth phase (Figure 3H), *e.g.*,

292   the biomarkers in stationary-phase with binary effects include glycogen (~1053 cm^{-1}),

293   Amide I (~1609 cm^{-1}), COO- symmetric stretching vibrations of fatty acids and

294   amino acid (~1389 cm^{-1}), asymmetric phosphate stretching vibrations ($v_{as}PO_2^-$; ~

295   1196 cm^{-1}), lipid (~ 1732 cm^{-1}), and Amide II (~1508 cm^{-1})[35, 60]. They change to

296   lipid (~1709 cm^{-1} and 1751 cm^{-1}), Amide I (~1609 cm^{-1}), Amide II (~1543 cm^{-1}),

297    $v_{as}PO_2^-$ (~1211 cm^{-1}) and glycogen (~1053 cm^{-1})[36, 60] in death-phase.

298   In general, most spectral alterations post-exposure are associated with lipids and

299   proteins indicating bacterial cell membranes are primary targets, probably because

300   tetracycline or AgNPs penetrate bacterial cells *via* passive diffusion and inhibits

301   bacterial growth by disturbing protein synthesis or altering membrane structure[63].

302   Through growth phases, Gram-negative bacteria inhibit a broad range of alterations

303   associated with lipids, *e.g.*, (1705 − 1750 cm^{-1}), which is absent in Gram-positive

304   bacteria, mainly attributed to their different cell wall composition. The rigidity and

305   extended cross-linking may reduce target sites on cell wall for environmental

306   exposure and increase difficulties in antimicrobial penetration[44].

307   *Factors influencing spectrochemical alteration*

308   From conducted spectral analysis, factors inducing IR spectral alterations can be

309   classified as intrinsic and external categories. The inherent one includes bacterial type

310   (Gram-positive or Gram-negative) and growth phase, and the external category refers

311   to the types of exposure. These factors function and interact simultaneously, with

312   distinct impacts on microbial responses to environmental exposures. To quantify the

313   importance of each factor, multivariate regression tree (MRT) analysis was conducted

314   through the isolated discriminating biomarkers (characteristic peaks). The MRT graph

315   illustrates the relationship of spectral variations and impact factors with four splits

316   according to bacterial types, growth phase and exposure groups, explaining 90.8% of

317   spectral variance (Figure 5).

318   Spectral variation is first split by bacterial type which accounts for 65.6% of the

319   total variation, owing to more changes associated with membrane components

320   observed in *P. fluorescens* (Gram-negative) than *M. vanbaalenii* (Gram-positive), *e.g.*,

321   proteins and phospholipid-derived fatty acids. Multivariate analysis also illustrates

322   various spectrochemical alterations between *P. fluorescens* and *M. vanbaalenii*. For

323   example, significant lipid changes (1705-1750 cm^{-1}) present in *P. fluorescens*

324   treatments are absent in *M. vanbaalenii* treatments. The cell membrane of

325   Gram-negative bacteria contains two lipid associated bilayers, which is likely to

326   increase the influence of applied exposure on the cell wall structure, while there is

327   only one lipid bilayer in the membrane and a thick ring of peptidoglycan and teichoic

328   acid of Gram-positive bacteria[17]. This difference may influence the structural integrity

329   and eventually the microbial response to external stimuli. Furthermore, both

330   Gram-positive and -negative bacteria from stationary phase show a comprehensive

331   range of alterations in cellular components (*i.e.*, Amide I, II, III, $v_{as}PO_2^-$/ $v_sPO_2^-$,

332   glycogen, carbohydrates, lipids, etc.; Figure 6), indicating many underlying biological

333   activities. This can be primarily attributed to a growing cell wall from log to

334   stationary phase, which increases the amounts of membrane components[64] and

335   induces changes on the surface of the bacterial envelope and protein synthesis[20]. Such

336   changes may have considerable influence on the rigidity of the cells, resistance to

337   environmental changes, as well as immunochemical properties. Results of both MRT

338   and multivariate analyses therefore suggest bacterial type as the primary intrinsic

339   factor determining IR alterations post-exposure to AgNP or tetracycline.

340   Growth phase also shows significant impacts on bacterial spectra after

341   environmental exposure. The Gram-negative group is further split in the MRT graph

342   by growth phase (*i.e.*, log-phase *vs.* stationary-phase and death-phase), owing to

343   increasing alterations of membrane components along with the growth stage, which

344   explains 13.2% of total variation (Figure 5). Similarly, multivariate analysis

345   demonstrates the same growth-dependent results. Post-exposure to AgNP for instance,

346   the spectra of both strains in log-phase are clearly separated from those in

347   stationary-phase or death-phase (Figure 2B-D). The induced alterations from growth

348   phases are associated with various cellular components. Specifically in log-phase, IR

349   spectral biomarkers reflecting the major alterations of *M. vanbaalenii* post-exposure

350   to AgNP are Amide I (~1612 cm^{-1}), COO- symmetric stretching vibrations of fatty

351   acids and amino acids (~1381 cm^{-1}), lipid (~1717 cm^{-1}), glycogen (~1011 cm^{-1}),

352    $v_{as}PO_2^-$ (~1215 cm^{-1}), and carbohydrate (~1165 cm^{-1}) (Figure 6A)[36, 60]. However,

353   samples from stationary-phase exhibit a contrasting profile consisting only of

354   alterations of proteins (~1377 cm^{-1}) and Amide I, II, III (~1609 cm^{-1}, 1566 cm^{-1}, 1254

355   cm^{-1}) (Figure 6B)[33]. In tetracycline or tetracycline-AgNP mixture treatments, the

356   most-induced biomarkers in log-phase shift to proteins, *i.e.*, Amide I (~1163 cm^{-1},

357   1616 cm^{-1}), Amide II (~1520 cm^{-1}, 1558 cm^{-1}) and Amide III (~1327 cm^{-1}) (Figure

358   6A)[33], but they are associated more with cellular components in stationary-phase,

359   including Amide I (~1589 cm^{-1}), Amide II (~1551 cm^{-1}), Amide III (~1269 cm^{-1}; 1273

360   cm^{-1}), proteins (~1485 cm^{-1}), lipid (~1717 cm^{-1}, 1721 cm^{-1}), COO- symmetric

361   stretching vibrations of fatty acids and amino acid (~1342 cm^{-1}; 1381 cm^{-1}), $v_sPO_2^-$

362   (~1069 cm^{-1}), $v_{as}PO_2^-$ (~1196 cm^{-1}) and glycogen (~1018 cm^{-1}) (Figure 6B)[60].

363   Samples from death-phase cultures exhibit distinct patterns as compared to log- or

364   stationary-phase in that AgNP and tetracycline-AgNP mixture show more impacts on

365   proteins (Figure 6C). These results indicate the changing physiological profiles of

366   bacterial cells with growth stage, and the different modifications associated with

367   cellular components with adaptation to the living environment. For instance, bacteria

368   facing nutrient depletion are reported to produce more hydrophobic molecules to

369   protect the starved cells, resulting in less fluid and permeable membranes attributed to

370   the transformations within the fatty acid composition, which increase protection and

371   insulation from a stressful environment[20, 61, 62]. Moreover, entering stationary phase, a

372   wide range of protein synthesis is also altered by the global gene regulatory network,

373   which tends to swap the core functions from metabolism or catabolism to the

374   maintenance of cellular viability[20], possibly explaining more spectral alterations of

375   proteins in stationary- and death-phase than log-phase.

376   Besides intrinsic factors, external environmental exposure explains 12.0% of total

377   variation in MRT for Gram-positive (2.7%) and Gram-negative (9.3%) bacteria. For

378   both strains, segregation mainly results from different spectrochemical alterations

379   between AgNP exposure and tetracycline/binary groups. The key spectral alterations

380   in the AgNP category are located at COO- symmetric stretching vibrations of fatty

381   acids and amino acid (~1373 cm^{-1}), (~1736 cm^{-1}), proteins (~984 cm^{-1}, 988 cm^{-1}),

382   Amide I (1612 cm^{-1}, 1694), Amide II (1543 cm^{-1}, 1562 cm^{-1}), and $v_sPO_2^-$ (1088 cm^{-1})

383   (Figure 3B and 3F)[36, 60]. In contrast, changes induced by tetracycline or

384   tetracycline-AgNP mixture are associated with COO- symmetric stretching vibrations

385   of fatty acids and amino acid (~1373 cm^{-1}), proteins (~984 cm^{-1}), lipids (~1697 cm^{-1};

386   1732 cm^{-1}), and Amide I, II (~1562 cm^{-1}, 1616 cm^{-1}) (Figure 3C and 3G)[60].

387   It can be concluded that AgNP-induced spectral changes are mainly associated

388   with proteins, whereas broader cellular components are affected post-exposure to

389   tetracycline or tetracycline-AgNP mixture. It might be explained by tetracycline

390   penetrating cells *via* passive diffusion, which alters bacterial growth by inhibiting

391   protein synthesis or destroying the membrane. Phospho-lipids or proteins are

392   therefore more significantly affected as the primary receptors of passively

393   accumulated tetracycline[63]. Although mechanisms of AgNP interacting with

394   cytoplasmic membranes and penetrating into cells remain unclear[58, 65], our data

395   suggest that AgNP-induced alterations might be derived from some specific active

396   sites interacting with AgNP, *e.g.*, sulfur-containing proteins following a similar

397   mechanism as thiol groups of respiratory chain proteins and transport proteins[66-68].

398   To further assess the impact of exposure, the inter-category multivariate distances

399   of each category were also evaluated. PCA-LDA scores plots that compare the

400   spectrochemical alterations of the two bacterial strains within the same growth phase

401   are shown in Figure 4. The results illustrate distinct clustering of tetracycline

402   exposure away from the control category, but not for AgNP categories, whereas the

403   binary group is located between AgNP and tetracycline categories. The spectral

404   differences of *M. vanbaalenii* between categories of control and binary exposure are

405   slightly reduced within 0.1 as compared to the tetracycline exposure category,

406   indicating that AgNP may confer the exposure effect of tetracycline. Similar

407   alterations are observed for *P. fluorescens*. Additionally, for both *M. vanbaalenii* and

408   *P. fluorescens*, the AgNP and tetracycline categories in the stationary- or death-phase

409 shift in an opposite direction from the control, and the binary exposure category
410 locates closer to the tetracycline exposure group than control or AgNP exposure. This
411 finding is supported by a range of identical alterations identified in both AgNP and
412 binary exposure groups from stationary-phase to death-phase (*i.e.*, lipids, Amide I, II,
413 III, $\nu_{as}PO_2^-/\nu_sPO_2^-$).

414 Additionally, the analysis of reactive oxygen species (ROS) was also conducted
415 to evaluate the exposure impacts by calculating the CySS-to-protein ratio, derived
416 from Raman spectra (Figure 7), which points to cellular ROS levels[34]. Interestingly,
417 comparing to control category, only tetracycline-binary exposure appears to increase
418 ROS level ($P < 0.05$), whereas the induction of AgNP and tetracycline exposure is not
419 significant. Previous studies report the independent mechanisms of antimicrobials on
420 the involvement of ROS[69, 70]. The results herein hint at no ROS generation from
421 individual AgNP or tetracycline exposure, and the spectrochemical alterations more
422 likely result from the direct inhibition of cell-wall assembly, protein synthesis and
423 DNA replication. In binary exposure, AgNP penetration across the cell membrane
424 might increase permeability and result in more tetracycline entering the bacterial cell,
425 consequently triggering a ROS response[44, 71-74].

426 **Conclusions**

427 The present study demonstrates that spectrochemical techniques coupled with
428 multivariate analysis are a robust tool for investigating the bacterial response to
429 environmental exposures, revealing biochemical information longnitudinally at
430 low-level exposures. This approach can be applied to characterize and assess bacterial
431 alterations effectively post-exposure to a tetracycline and/or AgNP through growth
432 phases and is potentially feasible for *in situ* interrogation of antimicrobial effects in
433 real-time. Deeper insights into biospectral alterations in non-log phases pertaining
434 nutrient depletion conditions, which fits better with the real-world scenario of
435 microcosms, uncovers the distinct changes of biochemical fingerprints across growth
436 periods, hinting at an underestimation of antimicrobial effects in previous studies.
437 Bacterial type is ranked as the primary factor affecting microbial response to
438 environmental stimuli by MRT analysis, followed by growth phase and types of
439 antimicrobials. These findings will help our better understanding of the real
440 interactions between microbes and low-level antimicrobials under natural
441 environmental conditions, *e.g.*, nutrient depletion.

442

Conflicts of interest

There are no conflicts of interest to declare.

445

Acknlowledgement

448

References

1. G. Hamscher, S. Sczesny, H. Höper and H. Nau, *Analytical Chemistry*, 2002, **74**, 1509-1518.

2. T. S. TA, *Quintessence Int.*, 1998, **29**, 223-229.

3. J. C. Chee-Sanford, R. I. Aminov, I. J. Krapac, N. Garrigues-Jeanjean and R. I. Mackie, *Applied and Environmental Microbiology*, 2001, **67**, 1494-1502.

4. L. Cantas, S. Q. Shah, L. M. Cavaco, C. M. Manaia, F. Walsh, M. Popowska, H. Garelick, H. Burgmann and H. Sorum, *Frontiers in Microbiology*, 2013, **4**, 96.

5. M. Tandukar, S. Oh, U. Tezel, K. T. Konstantinidis and S. G. Pavlostathis, *Environmental Science and Technology*, 2013, **47**, 9730-9738.

6. J. L. Martinez and F. Baquero, *Upsala Journal Medical Sciences*, 2014, **119**, 68-77.

7. H. H. Lara, N. V. Ayala-Núñez, L. d. C. Ixtepan Turrent and C. Rodríguez Padilla, *World Journal of Microbiology and Biotechnology*, 2009, **26**, 615-621.

8. R. J. Griffitt, N. J. Brown-Peterson, D. A. Savin, C. S. Manning, I. Boube, R. A. Ryan and M. Brouwer, *Environmental Toxicology and Chemistry*, 2012, **31**, 160-167.

9. Y. Kampmann, E. De Clerck, S. Kohn, D. Patchala, R. Langerock and J. Kreyenschmidt, *Journal of Applied Microbiology*, 2008, **104**, 1808-1814.

10. A. Gupta and S. Silver, *Nature Biotechnology*, 1998, **16**, 888-888.

11. O. I. Kalantzi, R. Hewitt, K. J. Ford, L. Cooper, R. E. Alcock, G. O. Thomas, J. A. Morris, T. J. McMillan, K. C. Jones and F. L. Martin, *Carcinogenesis*, 2004, **25**, 613-622.

12. J. L. Barber, M. J. Walsh, R. Hewitt, K. C. Jones and F. L. Martin, *Mutagenesis*, 2006, **21**, 351-360.

13. E. K. Costello, C. L. Lauber, M. Hamady, N. Fierer, J. I. Gordon and R. Knight, *Science*, 2009, **326**, 1694-1697.

478 14. C. L. Lauber, M. Hamady, R. Knight and N. Fierer, *Applied and Environmental Microbiology*, 2009, **75**, 5111-5120.

480 15. P. Marschner, C.-H. Yang, R. Lieberei and D. Crowley, *Soil Biology and Biochemistry*, 2001, **33**, 1437-1445.

482 16. M. Wietz, B. Wemheuer, H. Simon, H. A. Giebel, M. A. Seibt, R. Daniel, T. Brinkhoff and M. Simon, *Environmental Microbiology*, 2015, **17**, 3822-3831.

484 17. J. R. Morones, J. L. Elechiguerra, A. Camacho, K. Holt, J. B. Kouri, J. T. Ramirez and M. J. Yacaman, *Nanotechnology*, 2005, **16**, 2346-2353.

486 18. S. M. Ede, L. M. Hafner and P. M. Fredericks, *Applied Spectroscopy*, 2004, **58**, 317-322.

488 19. J. Monod, *Annual Reviews in Microbiology*, 1949, **3**, 371-394.

489 20. R. Kolter, D. A. Siegele and A. Tormo, *Annual Reviews in Microbiology*, 1993, **47**, 855-874.

491 21. F. Růžička, V. Holá, M. Votava, R. Tejkalová, R. Horvát, M. Heroldová and V. Woznicová, *Folia Microbiologica*, 2004, **49**, 596-600.

493 22. F. Ruzicka, M. Horka, V. Hola and M. Votava, *Journal of Microbiological Methods*, 2007, **68**, 530-535.

495 23. T. Mathur, S. Singhal, S. Khan, D. Upadhyay, T. Fatma and A. Rattan, *Indian Journal of Medical Microbiology*, 2006, **24**, 25.

497 24. D. Klug, F. Wallet, S. Kacet and R. J. Courcol, *Journal of Clinical Microbiology*, 2003, **41**, 3348-3350.

499 25. P. Vasudevan, M. K. M. Nair, T. Annamalai and K. S. Venkitanarayanan, *Veterinary Microbiology*, 2003, **92**, 179-185.

501 26. E. Muñoz-Atienza, C. Araújo, R. del Campo, P. E. Hernández, C. Herranz and L. M. Cintas, *LWT-Food Science and Technology*, 2016, **65**, 357-362.

503 27. F. C. Tenover, R. D. Arbeit, R. V. Goering, P. A. Mickelsen, B. E. Murray, D. H. Persing and B. Swaminathan, *Journal of Clinical Microbiology*, 1995, **33**, 2233.

506 28. E. E. Vaughan, F. Schut, H. Heilig, E. G. Zoetendal, W. M. de Vos and A. D. Akkermans, *Current Issues in Intestinal Microbiology*, 2000, **1**, 1-12.

508   29.   M. Espy, J. Uhl, L. Sloan, S. Buckwalter, M. Jones, E. Vetter, J. Yao, N.

509   Wengenack, J. Rosenblatt and F. Cockerill, *Clinical Microbiology Reviews*,

510   2006, **19**, 165-256.

511   30.   D. Klein, *Trends in Molecular Medicine*, 2002, **8**, 257-260.

512   31.   J. Heber, R. Sevenson and O. Boldman, *Science*, 1952, **116**, ll.

513   32.   K. Norris, *Journal of Hygiene*, 1959, **57**, 326-345.

514   33.   M. J. Baker, J. Trevisan, P. Bassan, R. Bhargava, H. J. Butler, K. M. Dorling,

515   P. R. Fielden, S. W. Fogarty, N. J. Fullwood, K. A. Heys, C. Hughes, P. Lasch,

516   P. L. Martin-Hirsch, B. Obinaju, G. D. Sockalingum, J. Sule-Suso, R. J.

517   Strong, M. J. Walsh, B. R. Wood, P. Gardner and F. L. Martin, *Nature*

518   *Protocols*, 2014, **9**, 1771-1791.

519   34.   J. Li, R. Strong, J. Trevisan, S. W. Fogarty, N. J. Fullwood, K. C. Jones and F.

520   L. Martin, *Environmental Science and Technology*, 2013, **47**, 10005-10011.

521   35.   F. L. Martin, J. G. Kelly, V. Llabjani, P. L. Martin-Hirsch, I. I. Patel, J.

522   Trevisan, N. J. Fullwood and M. J. Walsh, *Nature Protocols*, 2010, **5**,

523   1748-1760.

524   36.   K. A. Heys, M. J. Riding, R. J. Strong, R. F. Shore, M. G. Pereira, K. C. Jones,

525   K. T. Semple and F. L. Martin, *Analyst*, 2014, **139**, 896-905.

526   37.   J. Schmitt and H.-C. Flemming, *Int Biodeterior Biodegradation*, 1998, **41**,

527   1-11.

528   38.   A. Bosch, D. Serra, C. Prieto, J. Schmitt, D. Naumann and O. Yantorno,

529   *Applied Microbiology and Biotechnology*, 2006, **71**, 736-747.

530   39.   J. J. Ojeda, M. E. Romero-González, R. T. Bachmann, R. G. Edyvean and S.

531   A. Banwart, *Langmuir*, 2008, **24**, 4032-4040.

532   40.   S. J. Clarke, R. E. Littleford, W. E. Smith and R. Goodacre, *Analyst*, 2005,

533   **130**, 1019-1026.

534   41.   N. Pradhan, S. K. Pradhan, B. B. Nayak, P. S. Mukherjee, L. B. Sukla and B.

535   K. Mishra, *Research in Microbiology*, 2008, **159**, 557-561.

536   42.   I. Chopra and M. Roberts, *Microbiology and Molecular Biology Reviews*,

537   2001, **65**, 232-260.

538   43.   M. D. Barton, *Nutrition Research Reviews*, 2000, **13**, 279-299.

539   44.   A. M. Fayaz, K. Balaji, M. Girilal, R. Yadav, P. T. Kalaichelvan and R.

540   Venketesan, *Nanomedicine*, 2010, **6**, 103-109.

541   45.   P. Li, J. Li, C. Wu, Q. Wu and J. Li, *Nanotechnology*, 2005, **16**, 1912.

542   46.   S.-J. Kim, O. Kweon, R. C. Jones, J. P. Freeman, R. D. Edmondson and C. E.

543   Cerniglia, *Journal of Bacteriology*, 2007, **189**, 464-472.

544   47.   J.-S. Seo, Y.-S. Keum and Q. X. Li, *International Journal of Environmental

545   Research and Public Health*, 2009, **6**, 278-309.

546   48.   L. S. Thomashow and D. M. Weller, *Journal of Bacteriology*, 1988, **170**,

547   3499-3508.

548   49.   R. Hirsch, T. Ternes, K. Haberer and K.-L. Kratz, *Science of the Total

549   Environment*, 1999, **225**, 109-118.

550   50.   R. Hirsch, T. A. Ternes, K. Haberer, A. Mehlich, F. Ballwanz and K.-L. Kratz,

551   *Journal of Chromatography A*, 1998, **815**, 213-223.

552   51.   G. Artiaga, K. Ramos, L. Ramos, C. Cámara and M. Gómez-Gómez, *Food

553   Chemistry*, 2015, **166**, 76-85.

554   52.   T. Silva, L. R. Pokhrel, B. Dubey, T. M. Tolaymat, K. J. Maier and X. Liu,

555   *Science of the Total Environment*, 2014, **468**, 968-976.

556   53.   J. Trevisan, P. P. Angelov, A. D. Scott, P. L. Carmichael and F. L. Martin,

557   *Bioinformatics*, 2013, 29, 1095-1097.

558   54.   F. L. Martin, M. J. German, E. Wit, T. Fearn, N. Ragavan and H. M. Pollock,

559   *Journal of Computational Biology*, 2007, **14**, 1176-1184.

560   55.   M. Paraskevaidi, C. L. M. Morais, K. M. G. Lima, J. S. Snowden, J. A. Saxon,

561   A. M. T. Richardson, M. Jones, D. M. A. Mann, D. Allsop, P. L.

562   Martin-Hirsch and F. L. Martin, *Proceedings of the National Academy of

563   Sciences USA*, 2017, **114,** E7929-E7938.

564   56.   M. J. Riding, F. L. Martin, J. Trevisan, V. Llabjani, I. I. Patel, K. C. Jones and

565   K. T. Semple, *Environmental Pollution*, 2012, **163**, 226-234.

566   57.   J. Li, G. G. Ying, K. C. Jones and F. L. Martin, *Analyst*, 2015, **140**,

567   2687-2695.

568 58. I. Sondi and B. Salopek-Sondi, *J. Colloid Interface Sci.*, 2004, **275**, 177-182.

569 59. F. Pomati, A. G. Netting, D. Calamari and B. A. Neilan, *Aquatic Toxicology*,

570 2004, **67**, 387-396.

571 60. Z. Movasaghi, S. Rehman and D. I. ur Rehman, *Applied Spectroscopy Reviews*,

572 2008, **43**, 134-179.

573 61. J. C. Betts, P. T. Lukey, L. C. Robb, R. A. McAdam and K. Duncan,

574 *Molecular Microbiology*, 2002, **43**, 717-731.

575 62. T. Hampshire, S. Soneji, J. Bacon, B. W. James, J. Hinds, K. Laing, R. A.

576 Stabler, P. D. Marsh and P. D. Butcher, *Tuberculosis*, 2004, **84**, 228-238.

577 63. D. Schnappinger and W. Hillen, *Archives of Microbiology*, 1996, **165**,

578 359-369.

579 64. G. D. Shockman, J. J. Kolb and G. Toennies, *Journal of Biological Chemistry*,

580 1958, **230**, 961-977.

581 65. C. Marambio-Jones and E. M. Hoek, *Journal of Nanoparticle Research*, 2010,

582 **12**, 1531-1551.

583 66. O. Gordon, T. V. Slenters, P. S. Brunetto, A. E. Villaruz, D. E. Sturdevant, M.

584 Otto, R. Landmann and K. M. Fromm, *Antimicrobial Agents and*

585 *Chemotherapy*, 2010, **54**, 4208-4218.

586 67. A. J. Kowaltowski and A. E. Vercesi, *Free Radical Biology and Medicine*,

587 1999, **26**, 463-471.

588 68. J. F. Turrens, *Bioscience Reports*, 1997, **17**, 3-8.

589 69. Y. Liu and J. A. Imlay, *Science*, 2013, **339**, 1210-1213.

590 70. I. Keren, Y. Wu, J. Inocencio, L. R. Mulcahy and K. Lewis, *Science*, 2013,

591 **339**, 1213-1216.

592 71. H. H. Lara, N. V. Ayala-Núñez, L. d. C. Ixtepan Turrent and C. Rodríguez

593 Padilla, *World Journal of Microbiology and Biotechnology*, 2010, **26**,

594 615-621.

595 72. Z.-M. Xiu, J. Ma and P. J. Alvarez, *Environ Sci Technol*, 2011, **45**, 9003-9008.

596 73. J. R. Morones, J. L. Elechiguerra, A. Camacho, K. Holt, J. B. Kouri, J. T.

597 Ramírez and M. J. Yacaman, *Nanotechnology*, 2005, **16**, 2346.

598   74.   D. Trachootham, Y. Zhou, H. Zhang, Y. Demizu, Z. Chen, H. Pelicano, P. J.

599   Chiao, G. Achanta, R. B. Arlinghaus and J. Liu, *Cancer Cell*, 2006, **10**,

600   241-252.

601

602

Figure Cations

Figure 1. Growth curves of *M. vanbaalenii* (A) and *P. fluorescens* (B) under AgNP, tetracycline and AgNP-tetracycline binary exposures. The exposure concentrations were 4 μg/L for AgNP and 1 μg/L for tetracycline. IR spectral average of *M. vanbaalenii* (C) and *P. fluorescens* (D) in different exposure treatments. The groups of "Log control", "Log silver", "Log tet" and "Log binary" refer to samples collected at log-phase following treatments of control, silver, tetracycline and binary-exposure, respectively.

Figure 2. Exposure effects within different growth phases (scale range of Y axis: -0.2 ~ 0.2). The Y axis refers to the values of LD1. *M. vanbaalenii*: control (A), post-exposure to AgNP (B), post-exposure to tetracycline (C), and post-exposure to AgNP-tetracycline mixture (D). *P. fluorescens*: control (E), post-exposure to AgNP (F), post-exposure to tetracycline (G), and post-exposure to AgNP-tetracycline mixture (H).

Figure 3. Vector-cluster analysis of exposure effects within different growth phases. *M. vanbaalenii*: control (A), post-exposure to AgNP (B), post-exposure to tetracycline (C), and post-exposure to AgNP-tetracycline mixture (D). *P. fluorescens*: control (E), post-exposure to AgNP (F), post-exposure to tetracycline (G), and post-exposure to AgNP-tetracycline mixture (H).

Figure 4. Exposure effects within the same growth phase. The Y axis refers to the values of LD1 in range of -0.2 to 0.2. *M. vanbaalenii*: log-phase (A), stationary-phase (B), and death-phase (C). *P. fluorescens*: log-phase (D), stationary-phase (E), and death-phase (F).

Figure 5. Multivariate regression tree (MRT) analysis of environmental variables explaining the discriminating biomarkers. The scale of the sub-figures represents the alteration degree (1.0 refers to the average level). Blue bars for wavelengths representing proteins, yellow bars for phospholipid-derived fatty acids, and grey bars for other cellular components.

Figure 6. Vector-cluster analysis of exposure effects within the same growth phase. *M. vanbaalenii*: log-phase (A), stationary-phase (B), and death-phase (C). *P. fluorescens*: log-phase (D), stationary-phase (E), and death-phase (F).

634 **Figure 7.** Ratio of cysteine (CySS, 668 cm^{-1}) to protein (1447 cm^{-1}) derived from

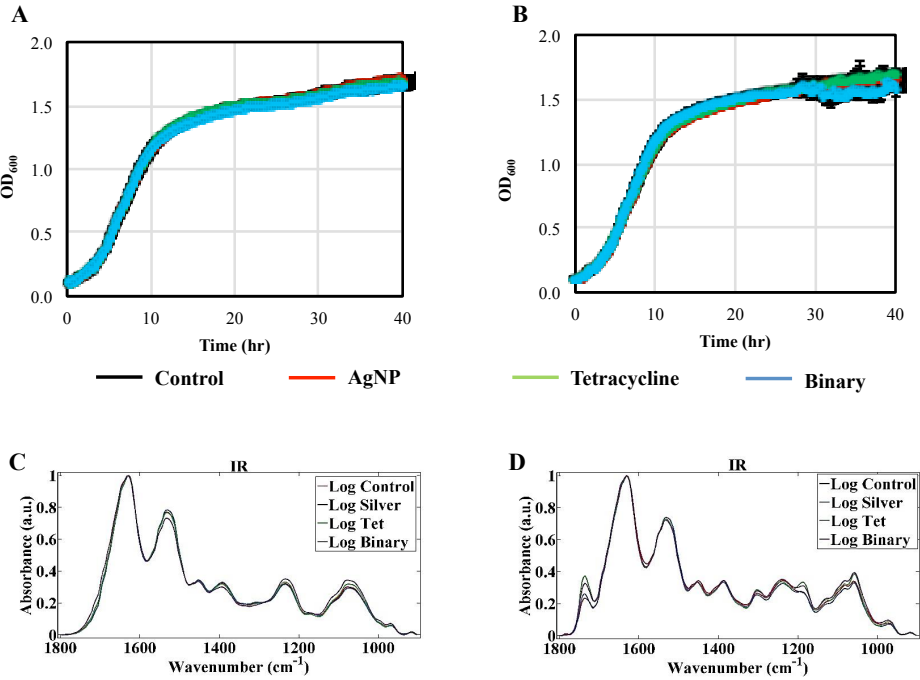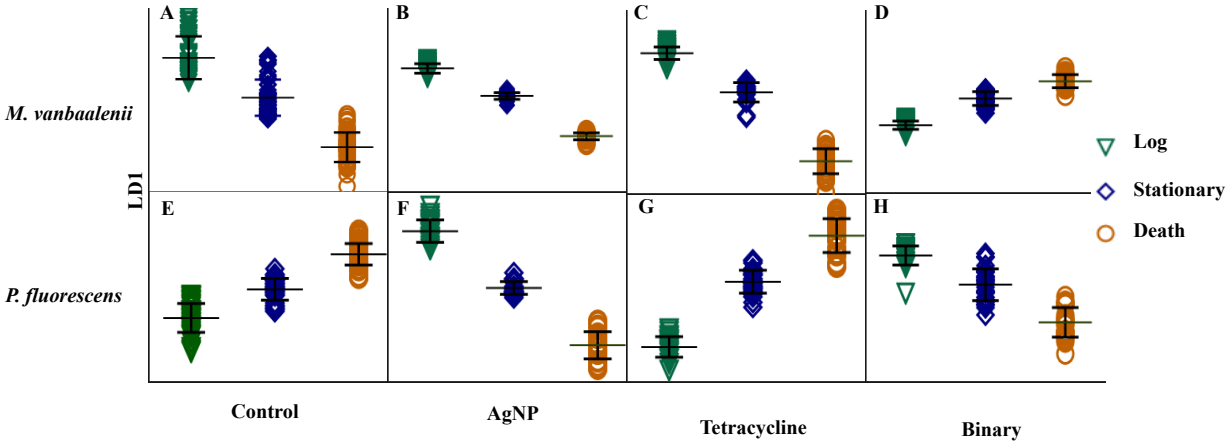635 Raman spectra. Data are presented in mean ± standard error.

636

637   **Figure 1**

638

A

639

B
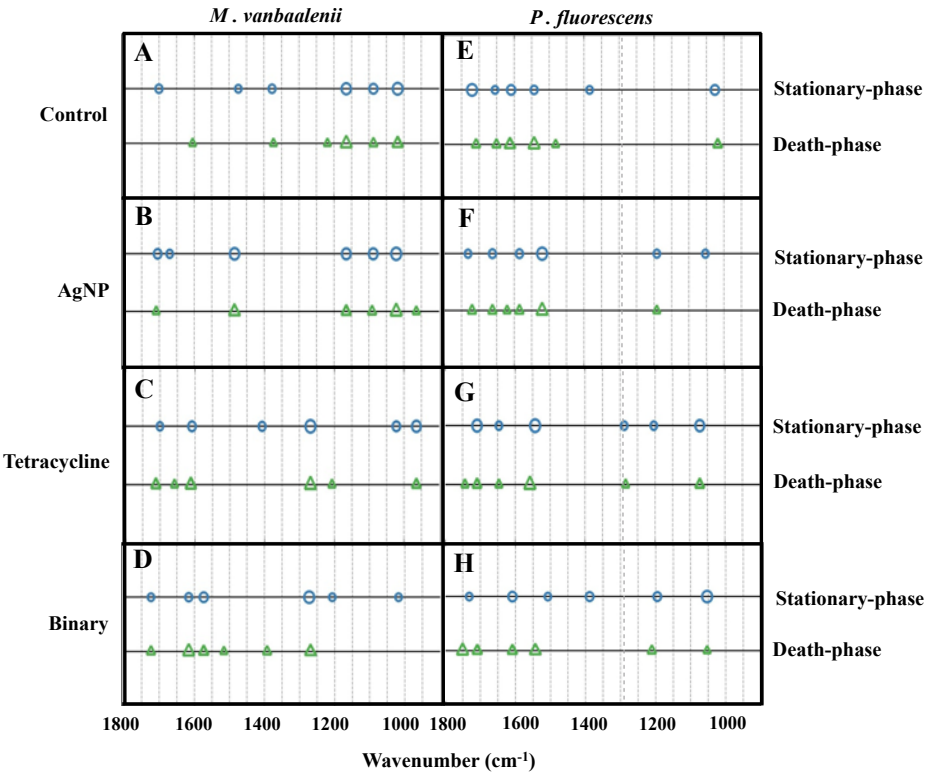
C

D

640

25

Figure 2

Figure 3

Figure 4

Figure 5

Figure 6

M. vanbaalenii   *P. fluorescens*

661 **Figure 7**

662

663